Bull. Mater. Sci., Vol. 40, No. 7, December 2017, pp. 1415–1420
https://doi.org/10.1007/s12034-017-1496-8

Unusual photoluminescence of Cu–ZnO and its correlation with photocatalytic reduction of Cr(VI)

S SHRAAVAN[1], SWAPNA CHALLAGULLA[2], SOURI BANERJEE[1] and SOUNAK ROY[2,*]

[1]Department of Physics, Birla Institute of Technology and Science (BITS) Pilani, Hyderabad Campus, Jawahar Nagar, Shameerpet Mandal, Hyderabad 500078, India

[2]Department of Chemistry, Birla Institute of Technology and Science (BITS) Pilani, Hyderabad Campus, Jawahar Nagar, Shameerpet Mandal, Hyderabad 500078, India

*Author for correspondence (sounak.roy@hyderabad.bits-pilani.ac.in)

MS received 29 November 2016; accepted 22 March 2017; published online 15 November 2017

Abstract. Cu–ZnO was synthesized by sol–gel route with a varied copper concentration of 1, 2 and 3 mol%. The synthesized materials were structurally characterized with powder X-ray diffraction and Raman spectroscopy, morphologically using a field emission scanning electron microscope, and electronic properties were studied with UV–visible spectroscopy and photoluminescence spectroscopy. Variation in Cu doping showed enhancement/quenching in photoluminescence of ZnO. This special characteristic is reflected in photocatalytic reduction of Cr(VI).

Keywords. Cu–ZnO; sol–gel synthesis; photoluminescence; photocatalytic reduction.

1. Introduction

Zinc oxide (ZnO) is an inexpensive, n-type, direct wide band gap II–VI semiconductor with optical transparency in the visible range. Substantial attention has been paid towards its application as a photocatalyst for vast usages, starting from a self-cleaning window to an advanced catalyst for wastewater treatment process [1–4]. The heterogeneous photocatalysis generally involves formation of an electron–hole pair upon suitable light irradiation. Catalytic oxidation is assumed to proceed directly by photogenerated holes (in valence band—VB) or by forming radicals, like $^{\bullet}OH$ and O_2^-, which are produced from surface adsorbed water, oxygen and hydroxyl groups. On the other hand, the photoexcited electrons in the conduction band (CB) help the catalytic reduction. The photocatalytic activity of ZnO can be improved by various techniques such as increasing the surface area [5], controlling the designed shape [6,7], doping a transition metal in the lattice [8] and so on. However, the major challenge in efficacy of a photocatalyst is the phenomenon like electron–hole recombination. Doping metals in ZnO have attracted attention for improving photocatalytic activities because it helps trapping the photo-induced charge carriers and (i) inhibits the charge recombination process, (ii) facilitates interfacial charge-transfer reaction and (iii) modifies the absorption spectrum of the metal oxide nanomaterials [9–17]. Ag doping in ZnO has been found to enhance the light absorption ability of ZnO nanomaterial as well as improve its gas sensing properties [18]. Since Ag is a very expensive metal, the development of a different low-cost metal for doping ZnO has been investigated in recent years. Cu is one of the metals of interest because it is in the same group as Ag and is widely used as a catalyst for many reactions. Also, Cu is a prominent luminescence activator in II–VI compounds; hence, it is quite significant that Cu-doped ZnO will exhibit possible modifications in physical and optical properties, which in turn influences the catalysis.

In this work, Cu–ZnO has been synthesized by sol–gel route [16] with a varied copper concentration of 1, 2 and 3%. The synthesized photocatalysts were used to photoreduce Cr(VI) to Cr(III) in aqueous solution. Cr(VI) is designated as one of the most priority pollutants present in waste and drinking water because of its acute carcinogenic and mutagenic nature to the living beings [19–21]. It is also reported that Cr(VI) can easily penetrate the placenta and affect the fetus [22,23]. On the other hand, Cr(III) is environmentally benign and also an essential metabolite for the functioning of insulin [24–28]. Therefore, as a model catalytic reaction, Cr(VI)–Cr(III) photoreduction was explored with Cu–ZnO oxides synthesized by the sol–gel route. The electronic properties of the synthesized catalysts were determined by photoluminescence (PL) and diffuse reflectance spectroscopy, and the results were correlated with their photocatalysis performances.

2. Experimental

Zinc acetate ($Zn(OAc)_2$) and copper acetate ($Cu(OAc)_2$) were purchased from SD Fine Chemicals and used as received.

S Shraavan and Swapna Challagulla have contributed equally to this study.

Diethanolamine (DEA), diphenyl carbazide (DPC) and isopropanol (IPA) were purchased from Alfa Aesar and used as received unless otherwise mentioned. The Cu-doped ZnO powders were prepared by the sol–gel method [16]. Requisite amount of $Cu(OAc)_2$ was dissolved in minimal amount of water, while requisite amount of $Zn(OAc)_2$ was dissolved in 20 ml of IPA. DEA was added to the $Zn(OAc)_2$ solution as a stabilizing agent. The Zn:DEA mole ratio was maintained as 1:1. The $Cu(OAc)_2$ solution was then added to the $Zn(OAc)_2$ solution and the resulting solution was stirred for 1 day at room temperature. This precursor solution was then aged for 1 day and the jelly-like substance was annealed at 800°C for 1 h to synthesize Cu–ZnO. The amount of $Cu(OAc)_2$ was varied to synthesize 1, 2 and 3 mol% Cu–ZnO.

X-ray diffraction (XRD) analysis with a Bruker AXS D8 Advance instrument was used for studying the crystalline property of the synthesized catalysts. The morphological study of as-synthesized catalysts was carried out using a field emission scanning electron microscope (FE-SEM, Carl-Zeiss ULTRA-55). Raman spectra were measured using a UniRAM 3300 Raman microscope with an incident laser wavelength of 532 nm. To study the band gap of the synthesized catalysts, solid-state UV measurements were performed with the help of a JASCO V-670 UV–visible spectrophotometer. PL measurements were carried out at room temperature, using a spectrofluorometer (JASCO FP-6300) at an excitation wavelength of 295 nm. A JASCO V-650 UV–visible spectrophotometer was used to analyse the Cr(VI) concentration during photocatalytic reduction.

The photoreduction of Cr(VI) was carried out in a cylindrical annular batch photoreactor fitted with a medium-pressure mercury vapour lamp of 125 W. The lamp was surrounded with a double-walled borosilicate immersion well and was constantly cooled by circulating water around it. For the photoreduction study, 20 ppm of 100 ml potassium dichromate solution, 4 mM oxalic acid and 30 mg of catalyst were taken in the reaction vessel. The pH of the solution was maintained at 3.0 using 0.1 M HCl and 0.1 M NaOH before starting the experiment. The solution was subjected to adsorption–desorption equilibrium under dark condition for 15 min. The aliquots were collected at regular time intervals during the photoreduction. The analysis of Cr(VI) was carried out by forming a complex with DPC and concentration was measured at 540 nm.

3. Results and discussion

Figure 1 shows the XRD patterns of pristine ZnO and Cu-doped ZnO powders. Pure ZnO was crystallized in a hexagonal wurtzite structure (JCPDS #75-0576). The crystallite size was determined using the Debye–Scherrer formula, $D = 0.9\lambda/\beta\cos\theta$, where D is the crystallite size, λ is the X-ray wavelength, β is the line width and θ is the angle of diffraction. The crystallite sizes of ZnO were found to be 53.6 nm. In the XRD pattern of 1% Cu–ZnO, there was no extra

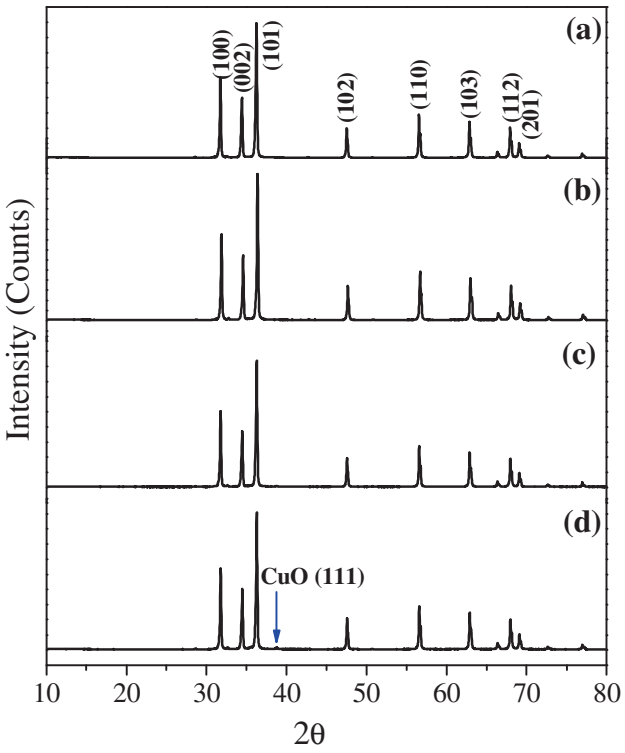

Figure 1. XRD patterns of (a) pristine ZnO, (b, c and d) 1, 2 and 3% Cu/ZnO, respectively.

peak due to CuO. This could be due to very high dispersion or low crystallinity of CuO or due to the lattice substitution of Cu. However, when Cu loading was increased to 2 or 3%, CuO (111) peak was observed at $2\theta = 38.78°$, and this indicates that with higher amount of Cu, it precipitates out of the solid solution. The crystallite size measured from XRD pattern was 51.7, 56.4 and 58.9 nm for 1, 2 and 3% Cu–ZnO, respectively. The crystallite size decreased in 1% Cu–ZnO compared with undoped ZnO. This was also observed in literature, due to formation of complex defects [29,30]. However, it is interesting to find out that with higher doping amount of Cu, the crystallite size increases.

Figure 2 presents the Raman spectroscopy of the synthesized catalysts. The space group C_{6v} describes the crystalline structure of the wurtzite ZnO compound with two formula units in the primitive cell. Optical phonons at the C point of the Brillouin zone belong to the irreducible representation $\Gamma(\text{optical}) = A_1 + 2E_2 + E_1$, where both A_1 and E_1 modes are polar and split into transverse optical (TO) and longitudinal optical (LO) phonons with different frequencies. Pristine ZnO showed a prominent peak at 436 cm^{-1} in addition to weak peaks at 330, 380 and 577 cm^{-1}. The peaks at 330, 380 and 578 cm^{-1} can be attributed to E_2(high)–E_2(low), A1(TO) and A1(LO) modes, respectively. The peak at 436 cm^{-1} can be attributed to Raman active modes of E_2(high), which represents the wurtzite hexagonal structure of ZnO [31,32]. This is in accordance with the XRD pattern of pristine ZnO. However, with Cu doping, there was a minor change in the E_2(high)

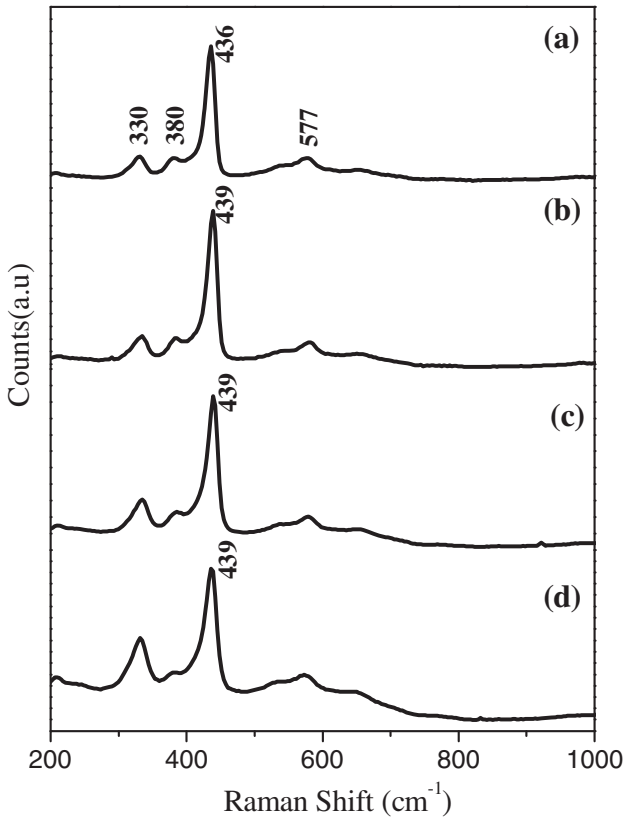

Figure 2. Raman spectroscopy of (a) pristine ZnO, (b, c and d) 1, 2 and 3% Cu/ZnO, respectively.

at 436 cm^{-1}. The band at 436 cm^{-1} in ZnO was shifted to 439 cm^{-1} in Cu–ZnO. Accordingly, the intensity was also influenced by the Cu doping. The intensity was weakened in 1% Cu–ZnO compared with ZnO; however, with higher doping the intensity was strengthened. This is in accordance with the literature [33].

Figure 3 presents the FE-SEM images of ZnO and Cu-loaded ZnO. The morphology of ZnO (figure 3a and b) was found to be cuboid shape, with smooth surface particles of size 80–100 nm. The Cu-loaded ZnO samples also showed similar morphology like ZnO with crystallite sizes ranging from 100 to 300 nm (figure 3c and h). There was no evidence of separate CuO particles, which may be due to very high dispersion or low crystallinity of CuO particles. The ED spectra confirmed the presence of Cu according to its loading.

The optical band structure of a semiconductor plays a pivotal role in determining its potential catalytic utility. $(KE)^{1/2}$ *vs.* E plots, derived from diffuse reflectance spectra of pristine ZnO, 1, 2, and 3% Cu–ZnO are shown in figure 4a. The Kubelka-Munk factor (K) is calculated using the formula $K = (1 - R)^2/2R$, where R represents the % reflectance and E is energy of the incident radiation. The pristine ZnO synthesized by the sol–gel route shows a direct semiconducting band gap (E_g) of 3.3 eV. With the introduction of Cu, the band gap was slightly reduced to 3.1 eV. However, by varying the Cu concentration, there was no significant difference in E_g. The narrowing of the band gap for Cu–ZnO compared with pristine ZnO could be due to the presence of Cu^{2+}(3d) band just below the CB of ZnO. Figure 4b describes the E_g between VB and CB of Cu–ZnO obtained from the diffuse reflectance spectra, which is merged with the standard reduction potential of Cr(VI)–Cr(III). Upon irradiation of UV light, the electrons move from the VB of ZnO to its CB, leaving the holes behind. The presence of Cu^{2+} may act as a heterojunction and the excited electron from the CB of ZnO may move downhill to the $Cu^{2+}(3d)$ band. This can reduce the electron–hole recombination. The photoexcited electron may reduce the Cr(VI) to Cr(III) efficiently.

PL spectra of pristine ZnO and Cu-doped ZnO powders are shown in figure 5. For the pristine and also for the doped oxides, there are two distinct emissions, one sharp peak at 335 nm, and a broad band at ~475 nm. Apparently, 1% Cu–ZnO showed enhanced UV emission and quenched visible

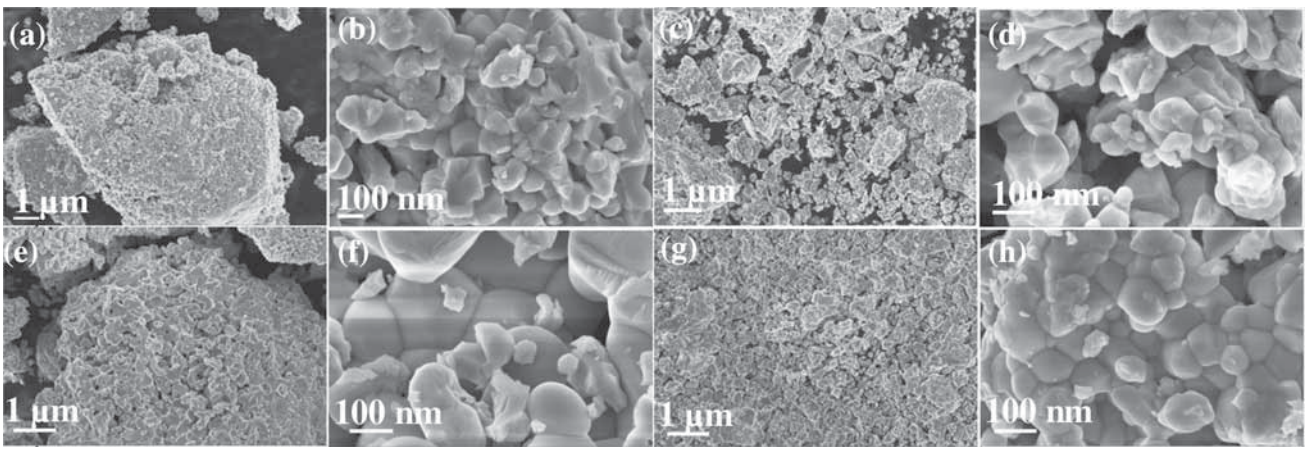

Figure 3. FE-SEM images of ZnO (**a**, **b**), 1% Cu/ZnO (**c**, **d**), 2% Cu/ZnO (**e**, **f**) and 3% Cu/ZnO (**g**, **h**).

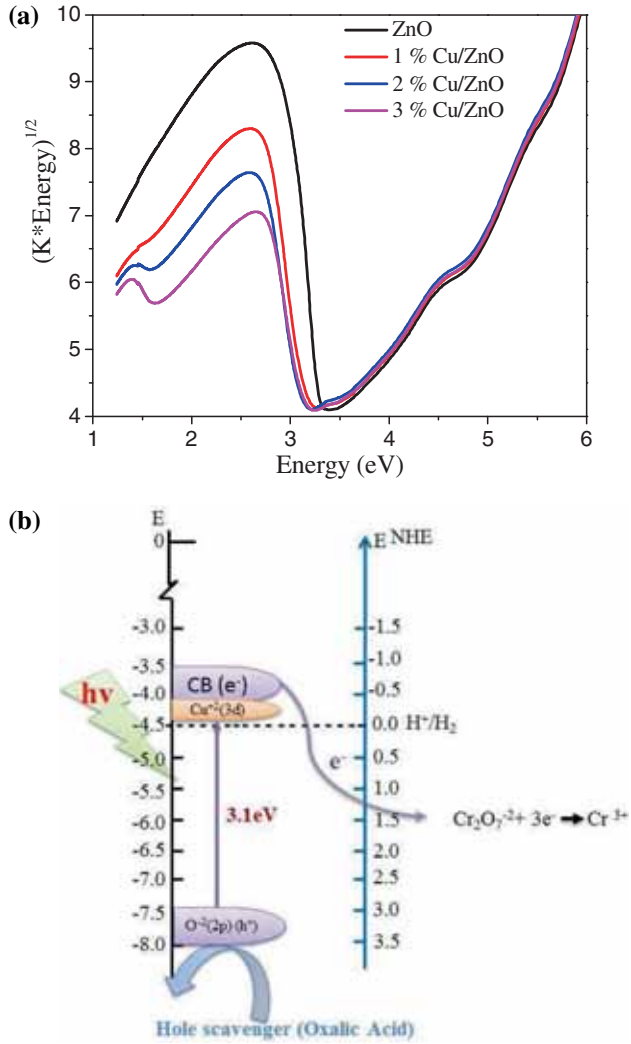

Figure 4. (**a**) Diffuse reflectance spectra of synthesized catalysts, and (**b**) the E_g between VB and CB of Cu/ZnO obtained from the diffuse reflectance spectra merged with reduction potential of Cr(VI).

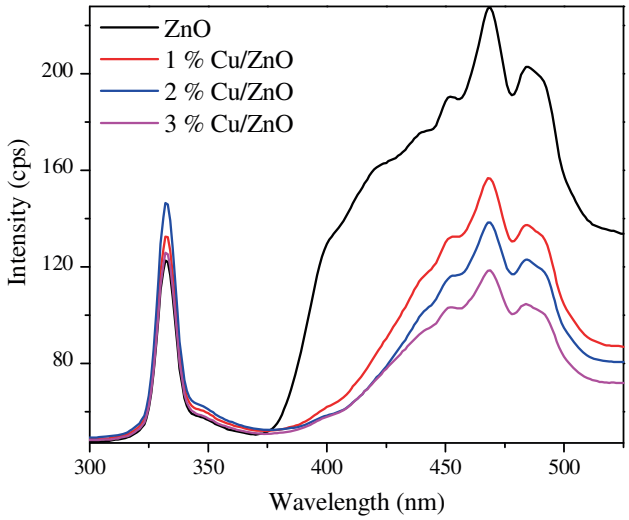

Figure 5. Photoluminescence spectra of pristine ZnO and Cu-doped ZnO powders.

emission compared with that of pristine ZnO. With increase in Cu doping, the visible emission is gradually quenched, but the UV emission shows some interesting behaviour. Compared with 1% Cu–ZnO, 2% Cu–ZnO showed enhanced UV emission; however, when the Cu concentration was increased to 3%, there was quenching in the emission peak; 2% Cu–ZnO showed the highest intensity of UV emission peak. It is known that the UV emission belongs to the band gap emission, while the visible emission is due to the defect emission that arises from the recombination of holes with electrons trapped at the oxygen vacancies in ZnO [34]. Generally, the lower PL intensity signifies lesser electron–hole recombination. It could be concluded from the PL spectra that higher Cu doping reduces the electron–hole recombination at the defect site; however, the recombination through direct band gap does not follow any linear trend.

The change in band gap and electron–hole recombination greatly influence the photocatalytic reactions. Therefore, photocatalytic reduction of Cr(VI) was explored with pristine and Cu-doped ZnO powders. Figure 6a shows the photoreduction of Cr(VI) in aerobic condition under UV light exposure against time. Oxalic acid was used as a hole scavenger for the photoreduction studies. As seen in the figure, the pristine ZnO reduced the Cr(VI) completely in 40 min, whereas, the doped Cu–ZnO required lesser time. Among the Cu-doped ZnO samples, 2% Cu–ZnO was the best and reduced Cr(VI) completely within only 25 min. The initial rates of the reactions were calculated at 10 min of progress of the reaction by the differential method in a batch reactor. The rate of the photoreduction over pristine ZnO and 1, 2 and 3% Cu–ZnO was found to be 4.3×10^{-2}, 5.09×10^{-2}, 7.98×10^{-2} and 5.62×10^{-2} mol l^{-1} g^{-1} min^{-1}, respectively. It should also be noted that 2% Cu–ZnO not only showed higher rate of Cr(VI) photoreduction, but also showed higher intensity in UV emission in PL compared with the other doped and undoped samples. For a constant volume of the reactor, the rate of the following catalytic reaction $\mathrm{Cr(VI)} \overset{\text{Catalyst}}{\rightarrow} \mathrm{Cr(III)}$ can be represented as follows:

$$\text{Rate} = -\frac{\mathrm{d}\,[\mathrm{Cr(VI)}]}{\mathrm{dt}} = \mathrm{k}[\mathrm{Cr(VI)}]^{\alpha},$$

$$\ln\left(\frac{\mathrm{d}\,[\mathrm{Cr(VI)}]}{\mathrm{dt}}\right) = \ln \mathrm{k} + \alpha \ln\,[\mathrm{Cr(VI)}]\,, \qquad (1)$$

where k is the rate constant and α is the order of the reaction. Equation (1) is plotted in figure 6b, and the rate constant for Cr(VI) photoreduction with 2% Cu–ZnO is found to be $1.18\ \mathrm{mol}^{1.205} \cdot \mathrm{L}^{-1.205} \cdot \mathrm{s}^{-1}$ with the order -0.205.

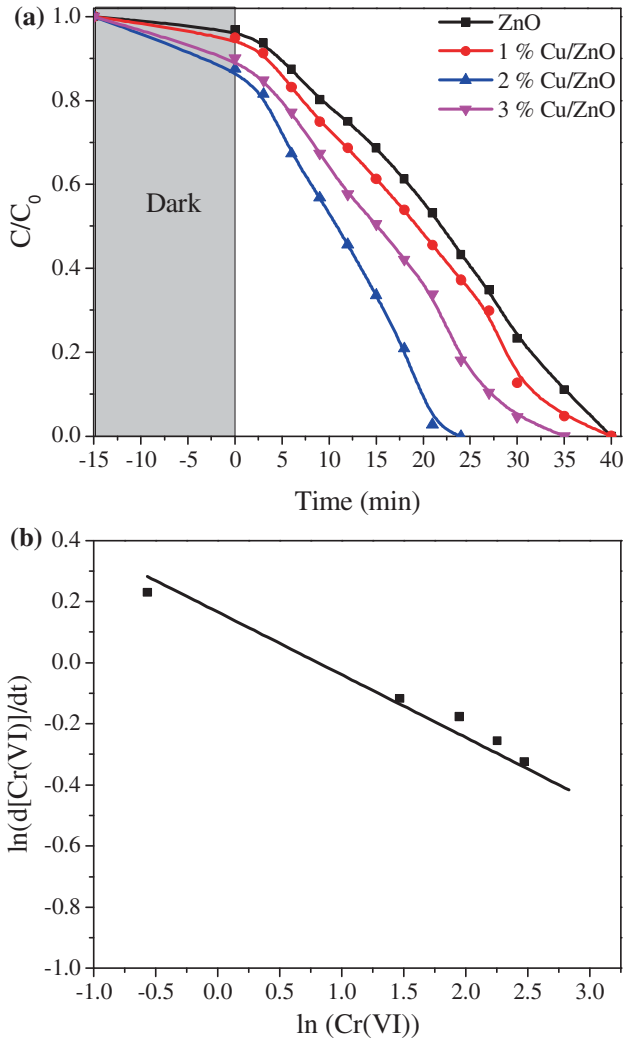

Figure 6. (**a**) Photoreduction of Cr(VI) with pristine ZnO and Cu-doped ZnO powders and (**b**) plot of ln[Cr(VI)] *vs.* ln(d[Cr(VI)]/dt) for Cr(VI) photoreduction with 2% Cu/ZnO.

4. Conclusion

Pristine ZnO and 1–3 mol% Cu–ZnO powders were synthesized by the sol–gel method. XRD analyses showed hexagonal wurtzite structure of the synthesized powders. CuO (111) peak was found only in 2 and 3% Cu–ZnO samples. Raman studies showed the evidences of Cu doping in ZnO. Band gaps of the materials were determined from diffuse reflectance spectra, which showed lowering of band gap due to Cu doping in ZnO. PL studies of the pristine and the doped materials showed interesting behaviour in electron–hole recombination, which was also reflected in photocatalytic reduction of Cr(VI).

Acknowledgement

SR thanks the Department of Science and Technology (SERB/F/825/2014-15) for the financial aid. The author also thanks BITS Pilani, Hyderabad Campus, for the Financial Assistance under 'Additional Competitive Research Grant'.

References

[1] Anandan S, Vinu A, Mori T, Gokulakrishnan N, Srinivasu P, Murugesan V *et al* 2007 *Catal. Commun.* **8** 1377
[2] Sheela T, Nayaka Y A, Viswanatha R, Basavanna S and Venkatesha T 2012 *Powder Technol.* **217** 163
[3] Chang S J, Hsueh T J, Chen I C and Huang B R 2008 *Nanotechnology* **19** 175502
[4] Law M, Greene L E, Johnson J C, Saykally R and Yang P 2005 *Nat. Mater.* **4** 455
[5] Ashe B 2011 Ph.D. Thesis, Department of Biotechnology & Medical Engineering, National Institute Of Technology, Rourkela, India
[6] Grasset F, Saito N, Li D, Park D, Sakaguchi I, Ohashi N *et al* 2003 *J. Alloys Compd*. **360** 298
[7] Hong R, Pan T, Qian J and Li H 2006 *Chem. Eng. J.* **119** 71
[8] Lima S, Sigoli F, Jafelicci Jr M and Davolos M R 2001 *Int. J. Inorg. Mater*. **3** 749
[9] Chauhan R, Kumar A and Chaudhary R P 2012 *Spectrochim. Acta Part A: Mol. Biomol. Spectrosc*. **98** 256
[10] Ekambaram S, Iikubo Y and Kudo A 2007 *J. Alloys Compd*. **433** 237
[11] Xiao Q and Ouyang L 2009 *J. Alloys Compd*. **479** L4
[12] Saleh R and Djaja N F 2014 *Spectrochim. Acta Part A: Mol. Biomol. Spectrosc*. **130** 581
[13] Ba-Abbad M M, Kadhum A A H, Mohamad A B, Takriff M S and Sopian K 2013 *Chemosphere* **91** 1604
[14] Chauhan R, Kumar A and Chaudhary R P 2012 *J. Sol–Gel Sci. Technol.* **63** 546
[15] Thongsuriwong K, Amornpitoksuk P and Suwanboon S 2012 *J. Sol-Gel Sci. Technol.* **62** 304
[16] Fu M, Li Y, Lu P, Liu J and Dong F 2011 *Appl. Surf. Sci.* **258** 1587
[17] Vijayalakshmi K and Karthick K 2014 *J. Mater. Sci. Mater. Electron.* **25** 832
[18] Li Y, Zhao X and Fan W 2011 *J. Phys. Chem. C* **115** 3552
[19] Nogueira A E, Lopes O F, Neto A B and Ribeiro C 2017 *Chem. Eng. J.* **312** 220
[20] Gaberell M, Chin Y P, Hug S J and Sulzberger B 2003 E*nviron. Sci. Technol.* **37** 4403
[21] Xie Q, Zhou H, Lv Z, Liu H and Guo H 2017 *J. Mater. Chem. A* **5** 6299
[22] Marouani N, Tebourbi O, Mokni M, Yacoubi M T, Sakly M, Benkhalifa M *et al* 2011 *Zygote* **19** 229
[23] Samuel J B, Stanley J A, Sekar P, Princess R A, Sebastian M S and Aruldhas M M 2014 *Environ. Toxicol.* **29** 814
[24] Xu S C, Ding H, Pan S, Luo Y and Li G 2016 *ACS Sustain. Chem. Eng.* **4** 6887
[25] Liu Y G, Hu X J, Wang H, Chen A W, Liu S M, Guo Y M *et al* 2013 *Chem. Eng. J.* **226** 131
[26] Mekatel H, Amokrane S, Bellal B, Trari M and Nibou D 2012 *Chem. Eng. J.* **200–202** 611
[27] Yang L, Xiao Y, Liu S, Li Y, Cai Q, Luo S *et al* 2010 *Appl. Catal. B: Environ.* **94** 142
[28] Yang C, Choi C H, Lee C S and Yi H 2013 *ACS Nano* **7** 5032

[29] Abinaya C, Marikkannan M, Manikandan M, Mayandi J, Suresh P, Shanmugaiah V *et al* 2016 *Mater. Chem. Phys.* **184** 172
[30] Chow L, Lupan O, Chai G, Khallaf H, Ono L, Cuenya B R *et al* 2013 *Sens. Actuators A: Phys.* **189** 399
[31] Thaweesaeng N, Supankit S, Techidheera W and Pecharapa W 2013 *Energy Procedia* **34** 682
[32] Zhang R, Yin P G, Wang N and Guo L 2009 *Solid State Sci.* **11** 865
[33] Wang X, Song C, Geng K, Zeng F and Pan F 2007 *Appl. Surf. Sci.* **253** 6905
[34] Heo Y, Norton D and Pearton S 2005 *J. Appl. Phys.* **98** 073502